Non-covalent interactions of Cysteine onto C60, C59Si, and C59Ge: A DFT study

Mohsen Doust Mohammadi
Tehran University: University of Tehran
hewa Y abdullah (hewayaseen@gmail.com)
Tishk International University https://orcid.org/0000-0001-5766-3858

Research Article

Keywords: Boron Nitride, Cysteine, C3H7NO2S, Density Functional Theory, Wave function analysis

Posted Date: August 10th, 2021

DOI: https://doi.org/10.21203/rs.3.rs-762620/v1

Version of Record: A version of this preprint was published at Journal of Molecular Modeling on October 28th, 2021. See the published version at https://doi.org/10.1007/s00894-021-04960-5.

Non-covalent interactions of Cysteine onto C_{60}, $C_{59}Si$, and $C_{59}Ge$: A DFT study

Mohsen Doust Mohammadi[a], Hewa Y. Abdullah[b,*]

[a] *School of Chemistry, College of Science, University of Tehran, Tehran 14176, Iran*

[b] *Physics Education Department, Faculty of Education, Tishk International University, Erbil, 44001, Iraq*

***corresponding author Email:** hewayaseen@gmail.com

Abstract

The study of intermolecular interactions is of great importance. This study attempted to quantitatively examine the interactions between Cysteine ($C_3H_7NO_2S$) and fullerene nanocages, C_{60}, in a vacuum. As the frequent introduction of elements as impurities into the structure of nanomaterials can increase the intensity of intermolecular interactions, nanocages doped with silicon and germanium have also been studied as adsorbents $C_{59}Si$ and $C_{59}Ge$. Quantum mechanical studies of such systems are possible in the density functional theory (DFT) framework. For this purpose, various functionals, such as B3LYP-D3, ωB97XD, and M062X, have been used. One of the most suitable basis functionals for the systems studied in this research is 6-311G (d), which has been used in both optimization calculations and calculations related to wave function analyses. The main part of this work is the study of various analyses that reveal the nature of the intermolecular interactions between the two components introduced above. The results of conceptual DFT, natural bond orbital, non-covalent interactions, and quantum theory of atoms in molecules were consistent and favored physical adsorption in all systems. Germanium had more adsorption energy than other dopants. The HOMO–LUMO energy gaps were as follows: C_{60}: 5.996, $C_{59}Si$: 5.309, and $C_{59}Ge$: 5.188 eV at B3LYP-D3/6-311G (d) model chemistry. The adsorption sensitivity increased when an amino acid molecule interacted with doped C_{60}, and this capability could be used to design a nanocarrier to detect Cysteine amino acids.

Keyword: Boron Nitride; Cysteine; $C_3H_7NO_2S$; Density Functional Theory; Wave function analysis.

Introduction

The first attempts to come up with the concept of intermolecular interactions were made by Clausius [1], van der Waals [2], and London [3,4]. Intermolecular interactions can be divided into long-range and short-range classes. The long-range class includes electrostatic, induction, and dispersion forces, and it varies with the inverse powers of the distance r^{-n}, which is the reciprocal of the intermolecular distance. Conversely, the short-range class includes exchange and repulsion forces that decrease exponentially with distance, as in $e^{-\alpha r}$. Both repulsive and attractive electrostatic forces arise from classical Coulombic interactions between the charge distributions of two molecules. These forces are also pairwise additive and anisotropic. The interacting molecules cause instantaneous fluctuations in the electron distribution, and such a disruption creates dispersion forces that are pairwise additive and always attractive. Induction forces, which are non-additive and attractive, are created by the distortion of the distribution of molecular charges resulting from the influence of the electric fields of other molecules. Exchange and repulsion are both non-additive and of opposite signs [5].

Ab initio calculations are a reliable method for obtaining polarizabilities (i.e., a set of constants to show the charge redistribution when a molecule is exposed to an electric field) and electric multipole moments used to explain the long-range forces [6]. In the case of short-range forces, the theory is rather more complicated [7] due to the overlap of electron densities between molecules. The previous long-range theory should be modified in terms of short-range penetration [8-10], charge transfer [11], and damping effects [12-14]. Generally, full quantum methods can only be well implemented in small systems, but there are technical problems with large molecules [15]. The development of wave function analysis methods has helped predict the nature of intermolecular interactions, even in the case of large systems. Although the ab initio

methods are few, neat, and classifiable, there are countless wave function analysis methods that have not yet been systematically categorized in the scientific literature.

After Feynman's famous "*There's Plenty of Room at the Bottom*" speech in 1959 in Caltech, the history of nanoscience has seen a dramatic expansion. Early works on carbon-based nanomaterials by Iijima [16,17] and Novoselov [18-21] paved the way for the development of nanotechnology in the use of inorganic nanomaterials. Among these, the structures of boron nitride are of special importance due to their extraordinary physical and chemical properties [22-24]. Studies on the optoelectrical, mechanical, and thermal properties [25] of such structures are still under consideration [26,27]. Furthermore, these nanomaterials are widely used, for example, as nanocarrier [28-39] or nanocarriers of drugs [40-42]. These processes occur through adsorption (adhesion of a particle to a surface), and they are primarily related to the intermolecular interactions between the adsorbent and the adsorbate.

This study examined the adsorption of Cysteine amino acid molecule onto the surface of pristine, silicon-, and germanium-doped fullerene nanocages, C_{60}, $C_{59}Si$, and $C_{59}Ge$, respectively. All structures, such as isolated species and complex systems, were optimized using various functionals, including B3LYP-D3, ωB97XD, M062X, and 6-311G(d) basis set. The most stable structure in terms of electronic energy was chosen for further wave function analyses using the B3LYP-D3/6-311G(d) model chemistry. We referred to the conceptual density functional theory (DFT), natural bond orbital (NBO), non-covalent interactions (NCI), and quantum theory of atoms in molecules (QTAIM) from among the most important and reliable wave function analyses ever developed. In this study, they were used to understand the nature of intermolecular interactions. All studies were performed in vacuum; therefore, the sensitivity and reactivity of the adsorbent were appreciated. The main ideas of each analysis were explained in

the shortest possible way, as these materials are scattered in the available resources, and it is a little difficult for beginners to have them together.

Computational details

The Kohn–Sham DFT framework was implemented in this study. Each structure, including amino acidand nanocages, was geometrically optimized in a vacuum using the so-called Berny geometry optimization algorithm developed by H. B. Schlegel in 1982 [43]. The PBE0 functional [44,45], which is the hybrid–exchange correlation form of the Perdew–Burke–Ernzerhof generalized gradient approximation (GGA) [46], meta-hybrid GGA functional M06-2X developed by the Truhlar group [47,48], the Head–Gordon group functional ωB97XD [49], which includes dispersion and long-range corrections, and the Becke 3-parameter Lee–Yang–Parr functional with Grimme dispersion correction B3LYP-D3 [50-52] were employed. The MC-311 or 6-311G (split-valence triple-zeta) basis set in the Gaussian package [53] has been developed by many individuals [54-62]. In the current work, the 6-311(d) basis set was used (i.e., d-type Cartesian–Gaussian polarization functions). Split-valence basis sets allow orbitals to alter the size but not the shape. When polarized functions are added to the basis sets, this limitation is removed by including orbitals with an angular momentum greater than what is needed for the ground state to depict each atom. This basis set is large enough and well able to simulate molecular orbitals. Data from benchmark studies also confirm this fact [63-67]. GaussView 6.0.16 [68] and ChemCraft [69] packages were used for building molecules. Linux-based Gaussian 16 software Rev. C.01 [53] was used for self-consistent field (SCF) calculations (as link 502). The default convergence criteria remained intact during the calculations. The SCF convergence was considered by comparing the maximum force and maximum displacement with the threshold values (0.00045 Hartree/Bohr and 0.0018 Bohr). Moreover, no symmetry

limitations were imposed on the optimization process. Wave function stability, frequency checks, and zero-point energy corrections (ZPECs) were considered to ensure the accuracy of the calculations. Stability calculations guarantee that this optimized electronic wave function may be minimal in the wave function space rather than a saddle point and that it is completely different from finding minima or saddle points on a nuclear potential energy surface. As the Gaussian software includes the NBO version 3.1 software [70-72] (as link 607), it is used to perform population analysis studies. The Multiwfn [73] package developed by Tian Lu is fed by formatted Gaussian checkpoint files for various wave function analyses. In this work, Multiwfn was used for NBO, NCI, and QTAIM studies. O'Boyle et al. developed the cclib and GaussSum [74] package to obtain the DOS diagrams.

To calculate the adsorption energy (E_{ads}) of the two molecules (nanocage and CYSTEINE), the following underlying relation is applied:

$$E_{ads} = E_{cage/\text{amino}} - E_{cage} - E_{\text{amino}} + \Delta E_{(BSSE)} + \Delta E_{(ZPE)} \quad (1)$$

where $E_{\text{cage/amino}}$ is the energy of the cluster, and E_{amino} and E_{cage} are the energies of the isolated amino acidand nanocage, respectively. The negative values of E_{ads} (i.e., exothermic adsorptions) show that the formed amino acid/nanocage cluster is stable. The electron density of each nucleus can be determined using a function centred on another nucleus. Therefore, in all structures, the quality of the basis set is not the same. This means that the basis set of one molecule can be effective in compensating for the violation of the basis set of another molecule. This effect is called the basis set superposition error (BSSE). There are two well-known methods for the BSSE correction, (1) chemical Hamiltonian approach (CHA) [75] and Boys and Bernardi's counterpoise (CP) correction procedure [76,77,15] which CP method is employed in this work:

$$\Delta E_{(BSSE)} = \Delta E_{cluster} - \Delta E_{cage}^{cluster} - \Delta E_{\text{amino}}^{cluster} \quad (2)$$

The ZPECs are calculated using Eq. 3:

$$\Delta E_{(ZPE)} = \Delta E_{cluster(ZPE)} - \Delta E_{cage(ZPE)} - \Delta E_{\text{amino}(ZPE)} \quad (3)$$

Result and discussion

3.1 Methodology

The DFT concept was initiated by Thomas [78], Fermi [79], and Dirac [80] in 1927–1930 using uniform electron amino acidenergy densities. In 1951, Slater [81] opened a new horizon, which Hohenberg, Kohn, and Sham [82,83] turned into a complete theory in 1964–1965. In DFT, the overall energy is shown in terms of the full electron density instead of the complicated *N* electron wave function. DFT is considered an exact theory (not a *model* like the Hartree–Fock model), but the approximations that are applied have caused it to fail; nevertheless, it is an efficient and usable tool [84]. The Hartree–Fock model and Kohn–Sham DFT are presented as follows [85,84]:

$$E_{HF} = V + \langle h\rho \rangle + 1/2 \langle \rho J(\rho) \rangle - 1/2 \langle \rho K(\rho) \rangle \quad (4)$$

$$E_{KS} = V + \langle h\rho \rangle + 1/2 \langle \rho J(\rho) \rangle + \underbrace{E_X[\rho] + E_C[\rho]}_{E_{XC}[\rho]} \quad (5)$$

where V is the nuclear repulsion energy, ρ is the density matrix, $\langle h\rho \rangle$ is the one-electron (kinetic plus potential) energy, $1/2\langle \rho J(\rho) \rangle$ is the classical electron repulsion, $-1/2\langle \rho K(\rho) \rangle$ is the exchange energy, $E_X[\rho]$ is the exchange functional, and $E_C[\rho]$ is the correlation functional. By comparing relations 4 and 5, in Kohn–Sham formalism, the Hartree–Fock model is essentially a special case of DFT, where $E_X[\rho] = -1/2<\rho K(\rho)>$ and $E_C[\rho] = 0$. Accordingly, in DFT, the methods differ in having different functionals E_X and E_C.

Unfortunately, exact functionals for exchange and correlation are not known; therefore, approximations have historically been developed to approach the real values of physical quantities, such as local-density approximation (LDA), generalized gradient approximations (GGA) [86,46], meta-GGA, and hyper-GGA. In this respect, a number of functionals include only the exchange part, such as Becke 88 (B88) [86] and Gill96 (G96) [87], and some of them include a pure correlation part, such as Vosko–Wilk-Nusair (VWN5) [88], Perdew 86 (P86) [89], Lee–Yang–Parr (LYP) [90], Perdew–Zunger (PZ81) [91], Cole–Perdew (CP) [92], and Perdew–Wang (PW92) [93]. Conversely, Becke 97 (B97) [94], Perdew–Burke–Ernzerhof (PBEPBE) [44], and Perdew–Wang 91 (PW91PW91) [95] are examples of exchange–correlation functionals (see Head-Gordon et al. article for a general overview of the types of functionals to a climb of Jacob's ladder [64]). The origine of the diferences among the $E_{XC}[\rho]$ arise from exchange-correlation holes (i.e. an exclusion area around electron or a "no-fly zone" which prevents other electron to penetrate, each functional has its own XC fingerprint).

In the present study, the hybrid functionals PBE0 and B3LYP-D3 were used. Note that the D3 in B3LYP-D3 refers to the D3 version of Grimme's dispersion with Becke–Johnson damping (GD3BJ) [52]. In hybrid functions, the exchange energy is divided into two parts to improve performance. The first part is the result of accurate calculations obtained from Hartree–Fock calculations, and the next part of the exchange energy is calculated using the DFT method. B3LYP uses three mixing parameters:

$$E_{XC} = A*E_X(LSDA) + (1-A)*E_X(HF) + B*\Delta E_X(B88) + E_C(VWN) + C*E_C(LYP) \quad (6)$$

and PBE0 consists of a 1:3 mixture of Hartree-Fock (HF) and DFT exchange energies:

$$E_{XC} = 0.25*E_X(HF) + 0.75*E_X(PBE) + E_C(PW91) \quad (7)$$

B3LYP has a weakness in considering charge transfer excitations, as it is not a long-range corrected functional [96]. This means that it uses a constant of 20% HF exchange for both short and long ranges. CAM-B3LYP [97] and ωB97XD are range-separated hybrid functionals [98] that are suitable for excitation energy calculations and conjugated systems [99]. ωB97XD is a range-separated version of the B97 functional with Grimme's D2 dispersion model (addition of an empirical $C_6 \cdot R^{-6}$ dispersion term). In short-range interactions, it comprises 22% HF exchange contributions and 100% HF in the long-range. A standard error function is implemented to describe the intermediate region using a range separation parameter (i.e., ω = 0.2–0.3 $Bohr^{-1}$) [100]. The range-separated term consists of two parts which splits the DFT exchange interaction as follows:

$$\frac{1}{r_{12}} = \frac{\alpha + \beta * erfc(\omega r_{12})}{r_{12}} + \frac{\alpha + \beta * erf(\omega r_{12})}{r_{12}} \quad ; \quad erfc \equiv 1 - erf \tag{8}$$

The first term in Eq. 8 shows short-range contribution which is singular and decays to zero on a length scale of ∼1/ω and the second term is related to non-singular long-range part. The *a* and *β* parameters allow HF-exchange and DFT exchange incorporate over whole range. M06-2X, a meta-hybrid GGA functional with double non-local exchange (2X) amounts, belongs to the M06 suite of functionals with 54% HF contributions, in which the non-interacting kinetic energy density is used as input to the functional and the electron density and its gradient [101]. This functional is well defined for systems with dispersion forces.

Geometric surveys

In the first step, molecular geometries were constructed using GussView software. The method of making nanocages is explained fully in the Help section of the software. Creating a Cysteine amino acid molecule does not take much effort, but for more certainty, geometry

related to amino acidmolecules was prepared using the PubChem online database [102]. At the beginning of the research, we chose models that were faster and less expensive. All structures, including isolated molecules and clusters, were initially examined using PBE0/6-311G(d) model. As our ultimate goal was to examine intermolecular forces, we used models that calculated intermolecular interactions more accurately. The optimization process was repeated with the same basis set and functionals M06-2X, B3LYP-D3, and ωB97XD. The chemistry of the different models varied within the trade-offs made between computational cost and accuracy.

Once geometric optimization was completed, the presence or absence of imaginary frequencies (i.e., frequencies that have negative values do not represent the minimum and actually represent a transition state) was examined. Thus, in each optimized structure, frequency calculations were performed. In the output file of the Gaussian software, the keyword Nimag was assigned for this purpose. A value of zero (Nimag = 0) means that there are no negative frequencies according to the number of negative eigenvalues of the Hessian matrix. Frequency calculations were performed to determine the ZPEC, which must be added to the total energy.

To study the interactions between nanocages and a amino acid molecule, a C_{60} cage with 1.45 Å bond length was selected. The optimized C60 structure was used to prepare a doped nanocage. For this purpose, doped nanocages were obtained by substituting silicon and germanium instead of carbon atom and they were re-optimized in the same optimization process.

Each nanocage is illustrated in Fig 1, which shows the position of the doped elements compared with the pure nanocage. The injection of the doped elements slightly changed the length of the bonds, indicating that the electronic structure was altered. These changes in the electronic structure led to differences in properties. Doping is a critical and successful strategy for detecting the properties of a nanomaterial as an adsorbent [103]. The dopants alter the

sensing properties by changing the HOMO-LUMO gap and morphology, creating more centres for amino acidinteraction on the adsorbent surface.

As shown in Fig 2, there are five sites on the nanocage that have the potential to absorb the amino acidmolecule. The top of the carbon atom is represented by T_1. The position of T_2 is related to the placement of the amino acidmolecule on top of the bond beween two hexagonal rings . The T_3 position is the placement of the amino acidmolecule on top of the bond beween hexagonal and pentagonal rings. The T_4 position is located above the hexagonal ring. And T_5 is on top of the pentagonal ring. Structurally, the Cysteine molecule has four heads, each of which can be placed on any of the five adsorption sites in C60 (Fig 3).

The starting point of the study is placing the amino acid molecule on the absorbent surface in different positions with different angles and distances and with different orientations and optimizing the whole cluster system. Finding the global minimum is the most challenging step of the study. Although we may never get it right away in the computing process, various strategies can be used to find many local minima and choose the most stable mode based on their quantitative value. If we have the full potential energy surface (PES) of two fragments, we can easily report the global minimum. However, having the PES requires thousands of calculations, which are practically impossible. The approach followed in this research is based on placing the amino acidmolecule on the adsorbent surface at different distances and orientations. For this purpose, a low-cost method, such as PM6, was used. Dozens of initial orientations were selected to achieve the most stable structure in terms of energy content. The PEB0/6-311G(d) model chemistry was used to optimize the obtained stable structure and repeat the process using the abovementioned functionals.

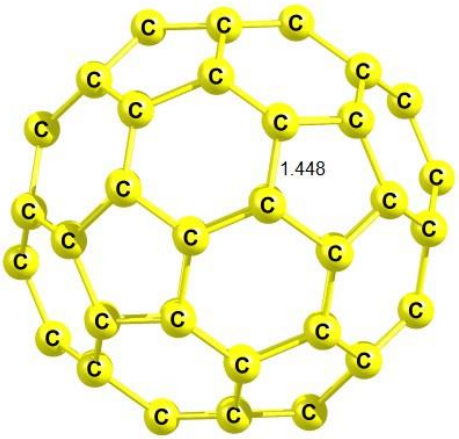

(a)

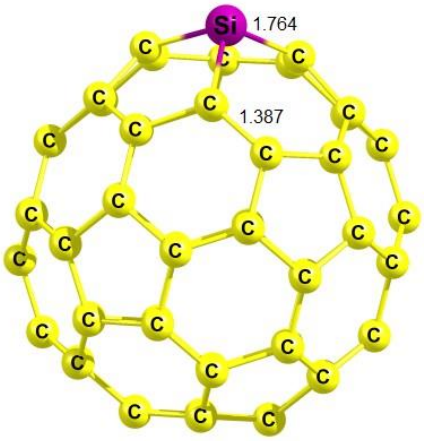

(b)

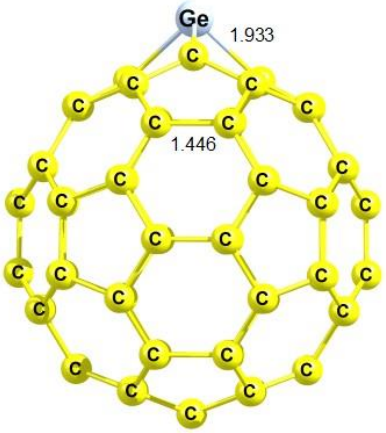

(c)

Fig 1. The values of bond length for (a) C_{60}, (b) $C_{59}Si$, and (c) $C_{59}Ge$. The optimization process has been done using the B3LYP-D3/6-311G (d) level of theory.

The relaxed cluster structures obtained from B3LYP-D3/6-311G (d) are illustrated in Fig 4. When the value of the energy of adsorption is below the range of chemical interest (i.e., from the third decimal place onwards following the decimal point), the results are identical [104]. Table 1 lists the values obtained from the calculations of the four different methods for optimizing complex structures. The quantitative amounts of adsorption energies obtained from the ωB97XD and B3LYP-D3 models were similar. Moreover, PBE0 data showed how different the data would be if the dispersion effect was not considered. Among the four different models, the values obtained from the B3LYP-D3/6-311G (d) model showed the highest stability, based on the absolute value of the highest absorption energy. As indicated in Table 1, among the doped elements, germanium produced the highest absorption energy (-1.121 eV).

To understand the nature of intermolecular forces, whether they are strong or weak or are the result of van der Waals or electrostatic effects, the wave function is analyzed in the following sections. According to Table 1 and based on our previous experience [105,106], the B3LYP-D3 functional is a better match to the systems studied in this paper. Thus, it was used for the wave function analysis calculations.

Table1

The interaction energy (E_{ads}) for C_{60}, $C_{59}Si$, and $C_{59}Ge$ with Cysteine molecule. All values are in (eV).

Systems	**PBE0**	**B3LYP-D3**	**M06-2X**	**ωB97XD**
Cysteine/C_{60}	-0.291	-0.555	-0.488	-0.520
Cysteine/$C_{59}Si$	-0.469	-0.629	-0.604	-0.677
Cysteine/$C_{59}Ge$	-0.773	-1.121	-0.957	-1.019

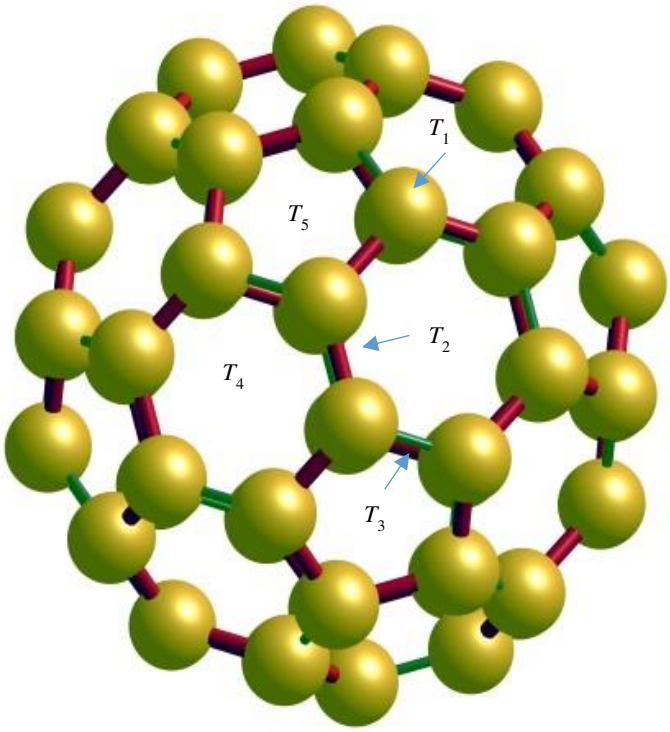

Fig 2. The (*T*x) positions including on top of carbon atom (T_1), on top of the bond beween two hexagonal rings (T_2), on top of the bond beween hexagonal and pentagonal rings (T_3), on top of the hexagonal ring (T_4), and top of the pentagonal ring (T_5).

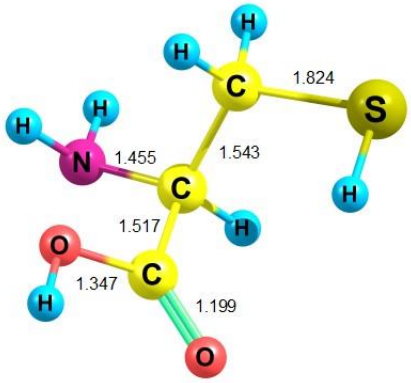

Fig 3. The values of bond length for Cysteine molecule. The optimization process has been done using the B3LYP-D3/6-311G (d) level of theory.

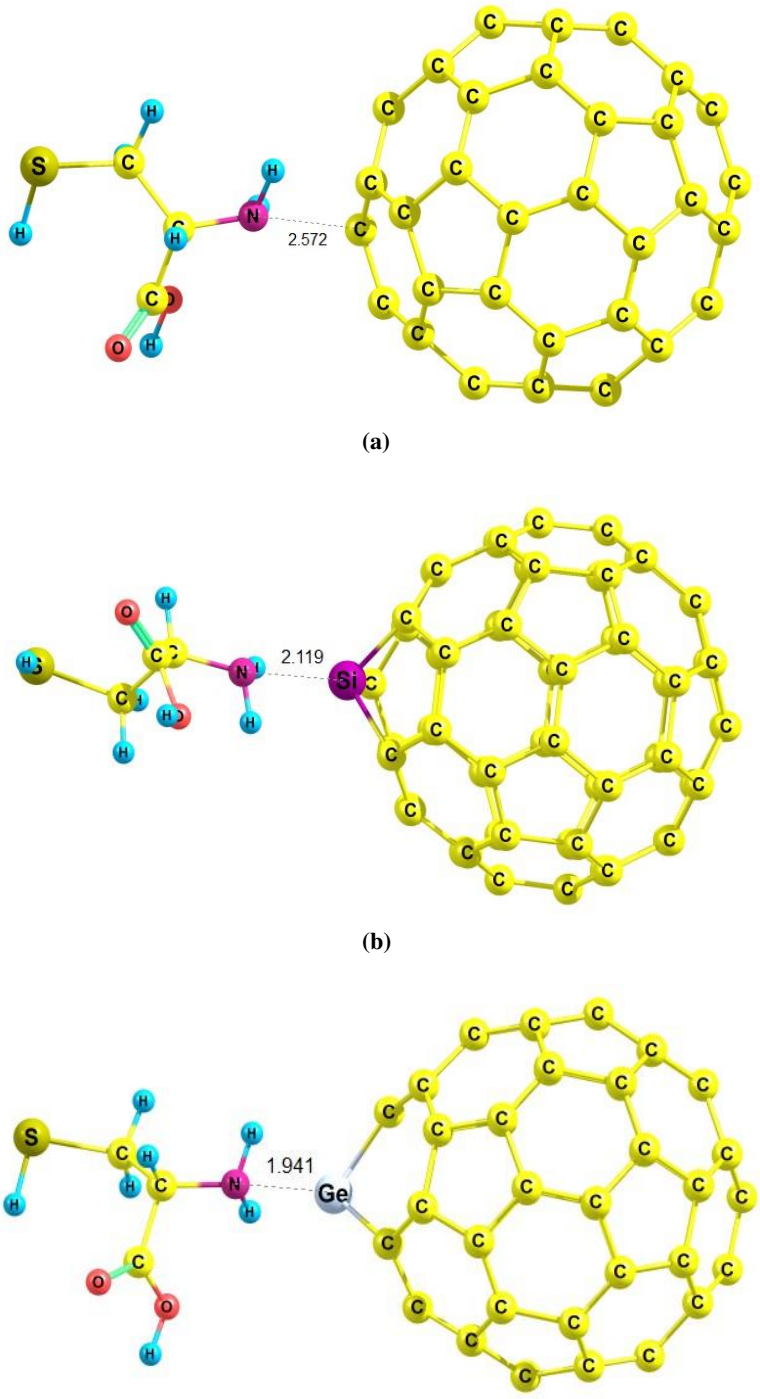

Fig 4. The most stable form of (a) Cysteine/C_{60}, (b) Cysteine/$C_{59}Si$, and (c) Cysteine/$C_{59}Ge$. All clusters have been optimized using the B3LYP-D3 functional and 6-311G(d) basis set.

Conceptual DFT descriptors

The conceptual DFT descriptors, including chemical potential (μ), chemical hardness (η), electronegativity (χ), electrophilicity (ω), and nucleophilicity ($1/\omega$), are implemented to consider the chemical reactivity/stability of certain atomic sites of molecules, the charge transfer through nucleophilic or electrophilic attacks, and the analysis of chemical reactions [107-109]. According to the basic principles of DFT, energy is a functional of the wave function (a functional can be used to turn a function into a number [110]), and the changes in the number of particles, ΔN, and external potential, $\Delta v(\mathbf{r})$, can describe a typical process. Therefore, if we have the ground state energy, $E[N, v(\mathbf{r})]$, of an N electron system, the energy of the perturbed system can be obtained as follows [111]:

$$\begin{aligned}\Delta E &\equiv E\left[N+\Delta N, v(\mathbf{r})+\Delta v(\mathbf{r})\right]-E\left[N, v(\mathbf{r})\right] \\ &=\left(\frac{\partial E}{\partial N}\right)_{v} \Delta N+\int\left(\frac{\delta E}{\delta v(\mathbf{r})}\right)_{N} \delta v(\mathbf{r}) d(\mathbf{r})+ \\ &\frac{1}{2!}\left\{\left(\frac{\partial^{2} E}{\partial N^{2}}\right)_{v} \Delta N^{2}+2 \int\left(\frac{\partial}{\partial N}\left(\frac{\delta E}{\partial v(\mathbf{r})}\right)_{N}\right)_{v} \Delta N \delta v(\mathbf{r})+\int \int\left(\frac{\partial^{2} E}{\partial v^{2}(\mathbf{r})}\right)_{N} \delta v(\mathbf{r}) \delta v(\mathbf{r}') d \mathbf{r} d \mathbf{r}'\right\}+\ldots\end{aligned} \tag{9}$$

The above Taylor expansion is usually truncated in the second order. The coefficients of the expansion have specific meanings in chemical language. For example, for non-degenerate states, perturbation theory describes electron density, $\rho(\mathbf{r})$, as follows [112,113]:

$$\left(\frac{\delta E}{\delta v(\mathbf{r})}\right)_{N}=\rho(\mathbf{r}) \tag{10}$$

Parr et al. [114] proved that μ is a quantitative measure of the tendency of an electron to pull out a system. The direction is from high to low μ values. The electronic chemical potential (μ) and electronegativity (χ) relation are expressed as Eq. 10

$$-\chi=\left(\frac{\partial E}{\partial N}\right)_{v(r)}=\mu \cong \frac{\left(\varepsilon_{LUMO}+\varepsilon_{HOMO}\right)}{2}=\frac{1}{2}(IP+EA) \tag{11}$$

Pearson [115] showed hardness (η) as a measure of resistance of a system to a change in the electronic cloud as follows:

$$\eta = \left(\frac{\partial \mu}{\partial N}\right) = \frac{1}{2}\left(\frac{\partial^2 E}{\partial N^2}\right)_{v(r)} = \frac{1}{2}\left(IP - EA\right) \tag{12}$$

Similarly, the Fukui function (which shows the change of $\rho(\mathbf{r})$ at a given position by changing of the number of electron, N) [116,117], f(r), and the dual descriptor [118], Δf(r) are defined as follows:

$$f(r) = \left(\frac{\delta^2 E}{\delta v(r) \partial N}\right) = \left(\frac{\partial \rho(r)}{\partial N}\right)_{v(r)} = \left(\frac{\partial \mu}{\delta v(r)}\right)_N \tag{13}$$

$$\Delta f(r) = \left(\frac{\delta^3 E}{\delta v(r) \partial^2 N}\right) = \left(\frac{\partial f(r)}{\partial N}\right)_{v(r)} = \left(\frac{\partial \eta}{\delta v(r)}\right)_N \tag{14}$$

Electrophilicity (ω) [119] is not the coefficient of the above-mentioned expansion. At the equilibrium point (μ = 0), ω is the stabilization energy gained by a system (i.e., ω is the capacity to accept an arbitrary number of electrons). In addition, a maximum number of electrons gained by the system $\Delta N_{\max}$ [120] prove that a typical system can be stabilized by gaining electrons when $\mu < 0$ and $\eta > 0$. Electrophilicity (ω) and $\Delta N_{\max}$ are defined as

$$\omega = \frac{\mu^2}{2\eta} \approx \frac{(IP + EA)^2}{4(IP - EA)} \tag{15}$$

$$\Delta N_{\max} = -\frac{\mu}{\eta} \tag{16}$$

As shown in the above equations, the HOMO–LUMO energy gap (HLG) [121] is related to ionization potential (IP) and electron affinity (EA). Theoretically, based on the Koopmans' [122] and Janak's [123] approximations, the ionization potential is equal to the negative value of HOMO, $(\varepsilon_{HOMO} = -IP)$, and the electron affinity is equal to the negative value of LUMO, $(\varepsilon_{LUMO} = -EA)$. It should be noted that HOMO and LUMO can only be obtained from HF or DFT (i.e single determinant methods) and the LUMO has no contribution to the total energy of

the system. In addition, calculating the LUMO values is basis set sensitive; however, methods have been developed that can eliminate the LUMO dependence on the basis set [124].

The values of these descriptors are presented in Table 2. The energy gap (E_g) of C60 was 5.996 eV using the B3LYP-D3/6-311G (d) model chemistry, and the adsorption of Cysteine on it reduced the energy gap to 5.067 eV. The silicon- and germanium-doped nanocages also reduced the HLG values. Molecules with large HLG had high values of η, whereas those with low HLG had low η. Table 2 shows that the LUMO values became more negative after the adsorption of Cysteine onto the nanocages; therefore, HLG was reduced. Reactivity of species was obvious due to the values of the descriptors η and μ. Conductivity arose from a high level of reactivity, and the charge transfer between the cages and adsorbate could be implemented through an chemical device as a carrier. To obtain a visual image of how the energy levels, especially HOMO and LUMO, are positioned, the total density of state maps is used in Fig 5.

Table 2

HOMO energy (ε_H), LUMO energy (ε_L), HOMO–LUMO energy gap (HLG), chemical potential (μ), chemical hardness (η), and electrophilicity (ω). All values are in eV and were obtained using the B3LYP-D3/6-311G (d) level of theory.

Systems	ε_H	ε_L	**HLG**	μ	η	ω
C_{60}	-8.176	-2.179	5.996	-5.177	2.998	40.183
$C_{59}Si$	-7.848	-2.540	5.309	-5.194	2.654	35.805
$C_{59}Ge$	-7.954	-2.766	5.188	-5.360	2.594	37.266
Cysteine/C_{60}	-6.705	-1.639	5.067	-4.172	2.533	22.045
Cysteine/$C_{59}Si$	-7.065	-1.783	5.282	-4.424	2.641	25.839
Cysteine/$C_{59}Ge$	-7.487	-2.428	5.059	-4.957	2.529	31.080

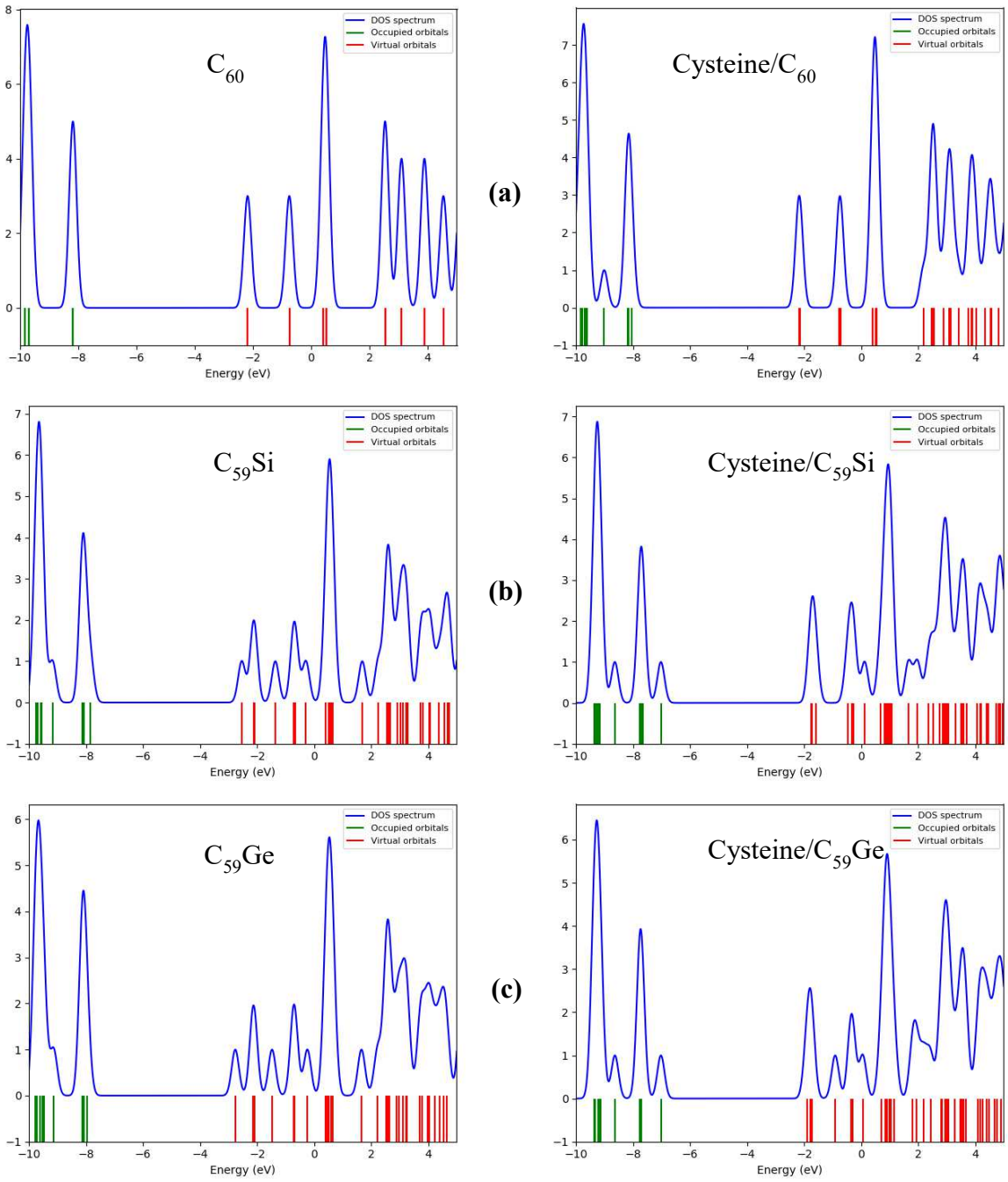

Fig 5. Density of state maps for (a) C_{60} and Cysteine/C_{60}, (b) $C_{59}Si$ and Cysteine/$C_{59}Si$, and (c) $C_{59}Ge$ and Cysteine/$C_{59}Ge$. Data were obtained from the B3LYP-D3/6-311G (d) model chemistry.

NBO analysis

Canonical molecular orbitals (MO) lead to delocalized descriptions of electrons derived directly from SCF methods [125]. Delocalization means that the MO obtained from several electrons belongs to adjacent atoms. As this is physically difficult to imagine, to create physical intuition, we had to use a method that would give us an understanding. As the wave function is invariant under unitary transformations, localization is possible. The NBO [70] method, developed by Weinhold et al., is an intuitive method used to reach localized and understandable orbitals (i.e., localized Lewis-like electronic structures) using the first-order reduced density matrix of the wave function.

Various types of NBO analyses offer tremendous power to display bond order, Lewis structures, donor–acceptor interactions, charge transfer, resonance weights, bond type, and hybridization. The validity of NBO analysis extends from atoms to supermolecules, spanning the entire periodic table. The term "natural" was introduced by Löwdin [126]. NBO analysis uses natural orbitals, as NBOs are obtained as local block eigenfunctions of the density matrix. "Bond orbital" means that the NBO algorithm calculates the distribution of electron density in bonds between atoms. Generally, NBO methods serve as a bridge between wave function and elementary valency and bonding concepts.

Providing a complete orthogonal set of natural atomic orbitals (NAOs), localized one-centre orbitals from the atom-centred basis set are the most fundamental parts of the NBO algorithm. To perform a natural population analysis, natural hybrid orbitals (NHOs), NBOs, and natural localized molecular orbitals (NLMOs) must be obtained from NAOs to transform a given wave function into localized orbitals that correspond to the one-centre ("lone pair") and two-centre ("bond") elements of the Lewis structure picture:

NAO → NHO → NBO → NLMO

For a (σ) bond located between atoms A and B, the NBO is defined as follows:

$$\sigma_{AB} = C_A h_A + C_B h_B \tag{17}$$

where C_A and C_B are the corresponding polarization coefficients (for covalent bonds $C_A = C_B$; if the electronegative A is assumed to be greater than B, we have: $C_A >> C_B$). The h_A and h_B are natural hybrid valance orbitals. To complete the span of valance space, an antibonding NBO (σ*) is also defined as follows:

$$\sigma^*_{AB} = C_A h_A - C_B h_B \tag{18}$$

In this study, NBO methods were utilized to measure the bond order. Coulson's definition of chemical bonding has paved the way for many chemical bond analyses [127]. The most popular methods used to find the bond order are the Mulliken bond order analysis [128] (Equation 19), the Mayer bond order [129-131] (Equation 20), and the Wiberg bond index (WBI) in Löwdin orthogonalized basis [132,133] (Equation 21). Therefore,

$$I_{AB} = \sum_i \eta_i \sum_{a\in A}\sum_{b\in B} 2C_{a,i}C_{b,i}S_{a,b} = 2\sum_{a\in A}\sum_{b\in B} P_{a,b}S_{a,b} \tag{19}$$

$$I_{AB} = I^{\alpha}_{AB} + I^{\beta}_{AB} = 2\sum_{a\in A}\sum_{b\in B}\left[\left(P^{\alpha}S\right)_{ba}\left(P^{\alpha}S\right)_{ab} + \left(P^{\beta}S\right)_{ba}\left(P^{\beta}S\right)_{ab}\right] \tag{20}$$

$$I_{AB} = \sum_{a\in A}\sum_{b\in B} P^2_{ab} \tag{21}$$

where P is the density matrix, and S is the overlap matrix. Compared with Mulliken and Mayer's bond orders, WBI has less basis set dependence, especially the basis set that includes diffuse functions, and it provides more accurate results. The WBI values are reported in Table 3. Accordingly, we can conclude that $C_{59}Si$ and $C_{59}Ge$ adsorbents are more active materials in this

study in adsorbing Cysteine compared with pristine C_{60}. The WBI values show that the interaction of the amino acidmolecule with C_{60} can be classified as a weak interaction. Conversely, the interactions between silicon- and germanium-doped C_{60} with the Cysteine molecule are stronger than the van der Waals interactions. The results of the WBI are in good agreement with the adsorption energies reported in Table 1.

Table 3

The, Mayer, Mulliken, and Wiberg bond index obtained for atomic bonds and intermolecular interactions between Cysteine molecule and C_{60}, $C_{59}Si$, and $C_{59}Ge$. All calculations were performed using the B3LYP-D3/6-311G(d) level of theory.

Systems	**Mulliken**	**Mayer**	**Wiberg**
Cysteine/C_{60}	0.039	0.088	0.201
Cysteine/$C_{59}Si$	0.232	0.298	0.450
Cysteine/$C_{59}Ge$	0.280	0.355	0.404

QTAIM analysis

The idea that a molecule is a collection of atoms linked by a network of bonds is not directly related to quantum mechanics and is beyond theoretical definition. Bader's topological quantum theory of atoms in molecules (QTAIM) analysis [134,135] was developed to answer the question, "*What is an atom in a molecule and how does one predict its properties*?" Based on the topology of the electron density, the structure of a molecule is revealed by the stationary points of the electron density and the gradient paths that originate and terminate at these points. In the AIM method, electrons are distributed in space in the gravitational field of the nucleus. This means that the nucleus exists as a point in a cloud of negative charge with an electron density distribution. Electron density $\rho(\mathbf{r})$ is a measurable property that determines the shape and properties of atoms and materials in general.

In this theory, a critical point is a minimum or a maximum of electron density ($\nabla\rho(\mathbf{r})=0$). A chemical bond is defined as a line between two atoms, in which the electron density is the maximum along with. There are trajectories that both originate and terminate at critical points and are related to each other by a saddle point. The nature of a critical point is defined by a Hessian matrix:

$$H_{ij} = \frac{\partial^2 \rho(r)}{\partial X_i \partial X_j} \tag{22}$$

$$\nabla^2 \rho(r) = \underbrace{\frac{\partial^2 \rho}{\partial x^2}}_{\lambda_1} + \underbrace{\frac{\partial^2 \rho}{\partial y^2}}_{\lambda_2} + \underbrace{\frac{\partial^2 \rho}{\partial z^2}}_{\lambda_3} \tag{23}$$

$$S = \sum_{i=1}^{3} Sign(\lambda_i) \tag{24}$$

where λ_i is the eigenvalue of the Hessian matrix. Critical points are identified by two characteristics: rank ($\lambda_i > 0$ or $\lambda_i < 0$) and signature ($\lambda_i \neq 0$). Critical points with a rank less than 3 are topologically unstable; thus, they become a number of critical points with a rank of 3. Using (R, S) coordinates, there are four types of critical points: *atomic critical point* (3,−3), *bond critical point* (BCP) (3, −1), *ring critical point* (RCP) (3,1), and *cage critical point* (CCP) (3,3) [136]. The following (Poincaré-Hopf) relation should be satisfied between critical points:

$$n - b + r - c = 1 \tag{25}$$

where n, b, r, and c denote the number of nuclei, BCP, RCP, and CCP, respectively. The Laplacian of electron density ($\nabla^2\rho(\mathbf{r}) = \lambda_1 + \lambda_2 + \lambda_3$) and that of electron density $\rho(\mathbf{r})$ at any BCP provide useful information about the different types of chemical interactions. The amount of $\rho(\mathbf{r})$ in BCP determines the bond strength and the bond order. In the case of the covalent bond, the Laplacian is less than zero ($\nabla^2\rho(\mathbf{r}) < 0$), and the values of $\rho(\mathbf{r})$ are large, indicating that the charges are concentrated between two nuclei. The positive values of the Laplacian ($\nabla^2\rho(\mathbf{r}) > 0$)

and the low values of $\rho(\mathbf{r})$ indicate that the charge dissipates in the distance between the two nuclei and that the interactions can be classified as a closed-shell type, which is related to ionic bonds, hydrogen bonds, and van der Waals bonds [137]. In particular, in the case of hydrogen bonding, if the electron density is in the range of 0.035–0.002 and if the Laplacian of electron density is in the range of 0.0139–0.002, the bond can be a hydrogen type.

The values of the Lagrangian kinetic energy $G(\mathbf{r})$, potential energy density $V(\mathbf{r})$, and energy density $H(\mathbf{r}) = G(\mathbf{r}) + V(\mathbf{r})$ can also be helpful in identifying the type of interactions. For a covalent bond, $H(\mathbf{r}) < 0$; $H(\mathbf{r})/\rho(\mathbf{r}) >> 0$; and $G(\mathbf{r})/|V|(\mathbf{r}) < 0.5$. For non-covalent interactions, $H(r) > 0$; $H(r)/\rho(r) > 0$; and $G(r)/|V|(r) > 1$. The virial theorem [138] suggests a relationship between $G(\mathbf{r})$, $V(\mathbf{r})$, and $\nabla^2\rho(\mathbf{r})$,

$$\frac{1}{4}\nabla^2\rho(\mathbf{r}) = 2G(\mathbf{r}) + V(\mathbf{r}) \tag{26}$$

Another descriptor is the bond elliptical index (ε), which is a good criterion for detecting conjugation and hyperconjugation. When ε is large, we have an elliptical structure that indicates that the π character is large. If $\varepsilon = 0$, the bond is cylindrical (double or triple) and very stable. Here, ε can be used to refer to the stability of the interactions and is defined as follows [139]:

$$\varepsilon = \frac{\lambda_1}{\lambda_2} - 1 \;;\quad \lambda_1 < \lambda_2 < 0;\ and\ \ \lambda_3 > 0 \tag{27}$$

Table 4

The AIM topological parameters, including electron density ($\rho(r)$), Laplacian of electron density ($\nabla^2\rho(\mathrm{r})$), the kinetic electron density $G(\mathrm{r})$, potential electron density $V(\mathrm{r})$, eigenvalues of Hessian matrix (λ), and bond ellipticity index (ε) at BCPs of the Cysteine molecule and C_{60}, $C_{59}Si$, and $C_{59}Ge$. All values have been calculated using the B3LYP-D3/6-311G(d) level of theory from NBO analysis.

Systems	ρ	$\nabla^2 r$	$G(\mathbf{r})$	$V(\mathbf{r})$	$G(\mathbf{r})/V(\mathbf{r})$	λ_1	λ_2	λ_3	ε
Cysteine/C_{60}	0.0332	0.1420	0.0348	-0.0341	1.0213	-0.0258	-0.0109	0.1787	1.3792
Cysteine/C_{59}Si	0.0542	0.0611	0.0375	-0.0597	0.6278	-0.0467	-0.0382	0.1460	0.2233
Cysteine/C_{59}Ge	0.0977	0.2660	0.1077	-0.1489	0.7234	-0.1120	-0.1156	0.4936	0.0316

Considering the values shown in Table 4, the Laplacian electron density $\nabla^2\rho(\mathbf{r})$ is positive for all interactions between the Cysteine amino acid molecule and all nanocages. Therefore, the interaction between amino acidand nanocages is detected as non-covalent. Fig 6 shows the BCP position. The presence of critical points between the amino acidmolecule and the nanocages emphasizes the strong interactions between the two components. Among the nanocages, $C_{59}Si$ and $C_{59}Ge$ are more capable of adsorbing the amino acidmolecule, as the values of $G(\mathbf{r})/|V|(\mathbf{r})$ for both of them are between 0.5 and 1. This means that the interaction tends to be strong in van der Waals. The other descriptors, $H(\mathbf{r})$ and $H(\mathbf{r})/\rho(\mathbf{r})$, agree with these results. The values obtained from ε show stable intermolecular interactions.

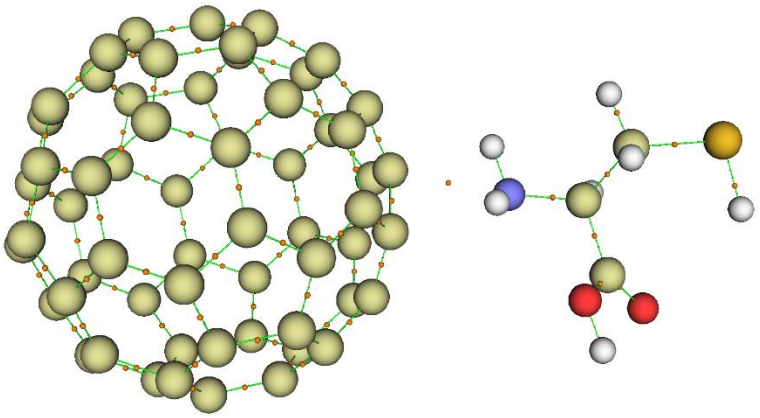

(a)

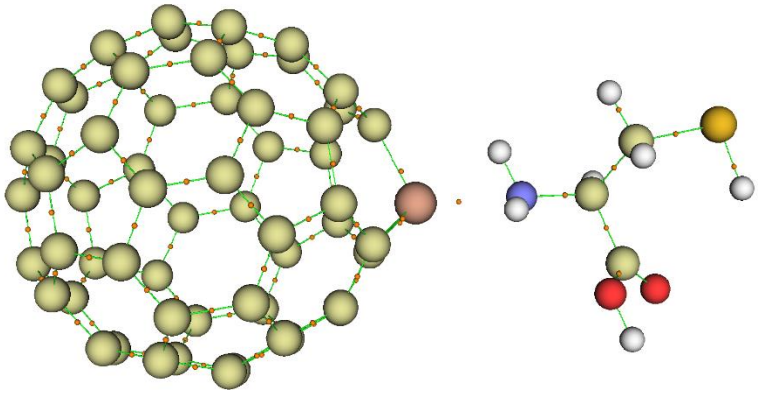

(b)

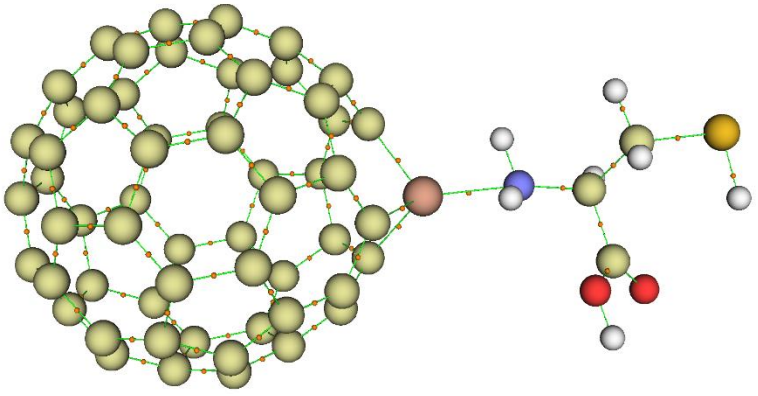

(c)

Fig 6. AIM molecular graphs for (a) Cysteine/C_{60}, (b) Cysteine/$C_{59}Si$, and (c) Cysteine/$C_{59}Ge$ systems. Orange dots represent the boundary critical points (BCPs).

NCI analysis

The results obtained from the previous sections show that the interactions between the amino acid molecule and pure and doped nanocages are non-covalent. Therefore, to verify this, these interactions were examined in terms of NCI analysis to determine the accuracy of the results. NCI analysis uses two functions: (1) $\mathrm{sign}\lambda_2(r)\rho(r)$ (product of electron density and the sign of the second Hessian eigenvector) and (2) reduced density gradient (RDG), which is a dimensionless form of a gradient of electron density [140]. The values of these two functions are displayed on a two-dimensional coordinate plane: the $\mathrm{sign}\lambda_2(r)\rho(r)$ is placed on the x-axis, and the RDGs are displayed on the vertical axis. The following equation is used to obtain the RDG values [140,141]:

$$RDG = \frac{1}{2(3\pi^2)^{\frac{1}{3}}} \frac{\left|\overline{\Delta\rho}(\mathbf{r})\right|}{\overline{\rho(\mathbf{r})}^{\frac{4}{3}}} \tag{28}$$

Depending on the position of the second function in the diagram, three areas are created, indicating the type of interactions. In the $\mathrm{sign}\lambda_2(\mathbf{r})\rho(\mathbf{r}) < 0$ region, strong non-covalent interactions are found; in the $\mathrm{sign}\lambda_2(\mathbf{r})\rho(\mathbf{r}) \approx 0$ region, relatively weak van der Waals interactions are defined; in the $\mathrm{sign}\lambda_2(\mathbf{r})\rho(\mathbf{r}) > 0$ region, repulsion forces are dominant [140,141]. Fig 7 compares the NCI plots for both isolated nanocages and amino acid/nanocages clusters. Repetitive results from previous analyses are also shown in the NCI analysis. That is, in the case of $C_{59}Si$ and $C_{59}Ge$ adsorbents, the adsorption intensity is stronger than in others. To reference this, $\mathrm{sign}\lambda_2(r)\rho(r) \approx 0$ and $RDG \approx 0.5$ should be considered.

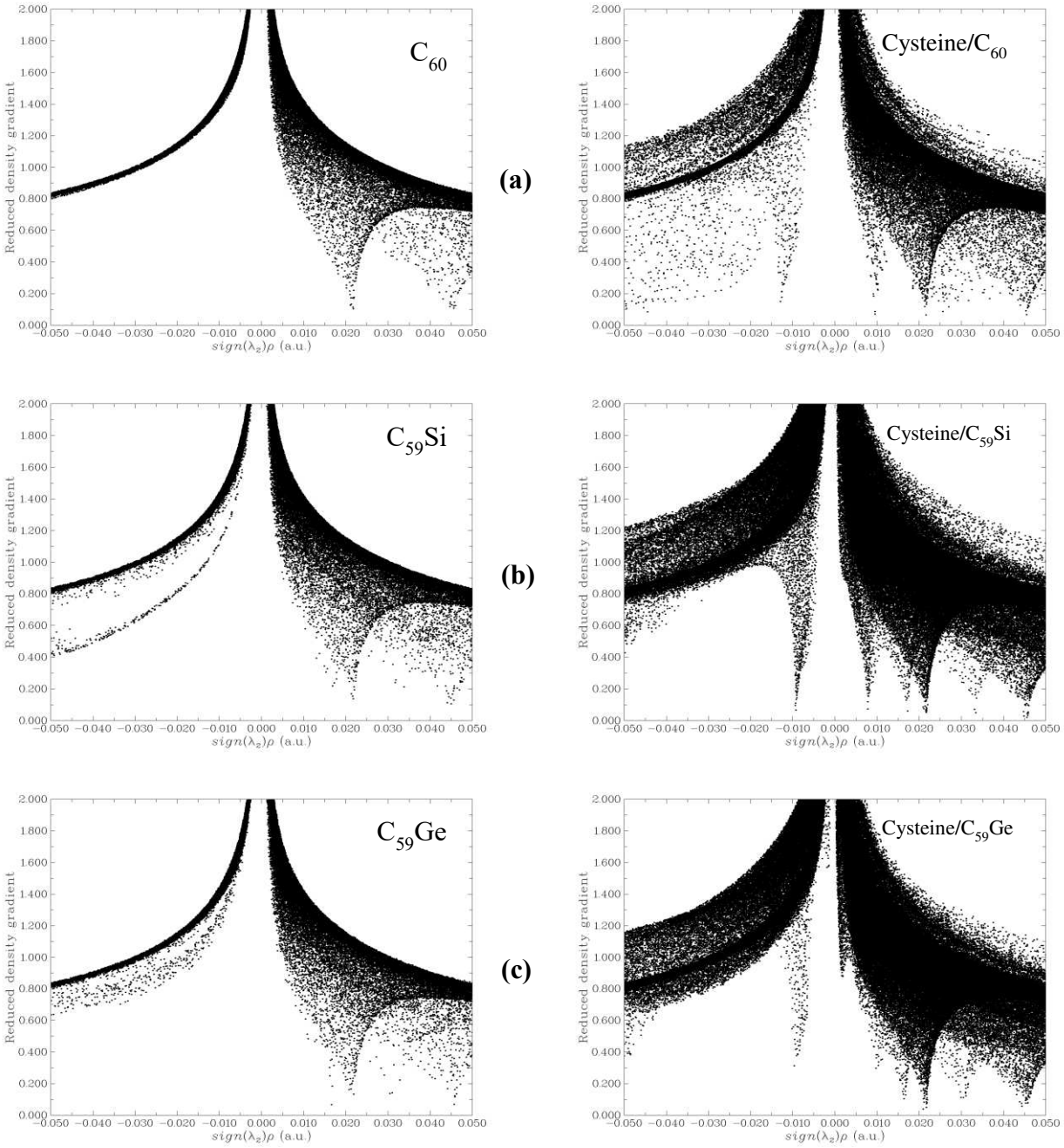

Fig 7. Plots for the reduced density gradient (RDG) vs. sign(λ_2)ρ(r) values of (a) C_{60} and Cysteine/C_{60}, (b) $C_{59}Si$ and Cysteine/$C_{59}Si$, and (c) $C_{59}Ge$ and Cysteine/$C_{59}Ge$. The data were obtained from B3LYP-D3 /6-311G (d) level of theory. The left side diagrams are isolated nanotubes and the right side diagrams are BCF/nanosheet clusters.

Conclusion

Various wave function analyses were performed to study the intermolecular interactions between the Cysteine amino acid and fullerene nanoadsorbents. The standard model chemistry in this study was B3LYP-D3/6-311G (d), which was implemented for the geometry optimization process and NBO calculations. The PBE0, ωB97XD, and M06-2X functionals and the 6-311G(d) basis set were also used for geometry optimization. Considering the dispersion in these functionals was a factor that completely changed the results of these calculations. In the optimization process, the spatial orientations of the two monomers relative to each other were the determining factors that led to the finding of the local minima. Spanning the entire potential energy surface for such interactions could not be attained. Therefore, it is important to use an appropriate algorithm to find the local minima. Comparing the adsorption energy of different clusters showed that the adsorbents $C_{59}Si$ and $C_{59}Ge$ trapped the amino acid molecule more intensely. The QTAIM and NCI analysis results identified the intermolecular interactions of the type of strong van der Waals interaction for these nanocages. As the amino acid and the mentioned adsorbents interacted well, these nanomaterials could be used to design a nanocarrier for the Cysteine molecule.

Acknowledgments

We would like to thank the Solid-State Theory Group at the Physics Department at the Universita‘ Degli Studi di Milano-Italy for providing computational facilities.

Conflict of Interest

The authors declare no conflict of interest

*Declarations

Funding: (Not)
Conflicts of interest/Competing interests: (Not)
Availability of data and material: (Not)
Code availability: (Gaussian 16)
Authors' contributions: (**Mohsen Doust Mohammadi**: Investigation, Writing - originaldraft. **Hewa Y. Abdullah**: Conceptualization, Writing - review & editing, Resources, Supervision.)

Reference

1. Clausius R (1857) Ueber die Art der Bewegung, welche wir Wärme nennen. Annalen der Physik 176 (3):353-380
2. Van der Waals JD (1873) Over de Continuiteit van den Gas-en Vloeistoftoestand, vol 1. Sijthoff,
3. London F (1930) Zur theorie und systematik der molekularkräfte. Zeitschrift für Physik 63 (3-4):245-279
4. London F (1937) The general theory of molecular forces. Transactions of the Faraday Society 33:8b-26
5. Spencer ND, Moore JH (2001) Encyclopedia of chemical physics and physical chemistry: Applications, vol 3. Taylor & Francis,
6. Dykstra CE (1988) Ab initio Calculation of the Structures and Properties of Molecules. Studies in physical and theoretical chemistry (58)
7. Elrod MJ, Saykally RJ (1994) Many-body effects in intermolecular forces. Chemical reviews 94 (7):1975-1997
8. Stone AJ (1996) The theory of intermolecular forces, Clarendon. Oxford Stone AJ, Alderton M (1985) Distributed multipole analysis–methods and applications Mol Phys 56:1047-1064
9. Hayes I, Stone A (1984) An intermolecular perturbation theory for the region of moderate overlap. Molecular Physics 53 (1):83-105
10. Jeziorski B, Moszynski R, Szalewicz K (1994) Perturbation theory approach to intermolecular potential energy surfaces of van der Waals complexes. Chemical Reviews 94 (7):1887-1930
11. Stone AJ (1993) Computation of charge-transfer energies by perturbation theory. Chemical physics letters 211 (1):101-109
12. Kreek H, Meath WJ (1969) Charge-Overlap Effects. Dispersion and Induction Forces. The Journal of Chemical Physics 50 (6):2289-2302
13. Knowles PJ, Meath WJ (1986) Non-expanded dispersion and induction energies, and damping functions, for molecular interactions with application to HF-He. Molecular Physics 59 (5):965-984
14. Wheatley RJ, Meath WJ (1994) Induction and dispersion damping functions, and their relative scale with interspecies distance, for (H+, He+, Li+)-(H, He, Li) interactions. Chemical physics 179 (3):341-364
15. Van Duijneveldt FB, van Duijneveldt-van de Rijdt JG, van Lenthe JH (1994) State of the art in counterpoise theory. Chemical Reviews 94 (7):1873-1885
16. Iijima S (1991) Helical microtubules of graphitic carbon. nature 354 (6348):56-58
17. Iijima S, Ichihashi T (1993) Single-shell carbon nanotubes of 1-nm diameter. nature 363 (6430):603-605
18. Geim AK, Novoselov KS (2010) The rise of graphene. In: Nanoscience and technology: a collection of reviews from nature journals. World Scientific, pp 11-19
19. Novoselov KS, Geim AK, Morozov SV, Jiang D, Katsnelson MI, Grigorieva I, Dubonos S, Firsov, AA (2005) Two-dimensional gas of massless Dirac fermions in graphene. nature 438 (7065):197-200

20. Novoselov KS, Geim AK, Morozov SV, Jiang D, Zhang Y, Dubonos SV, Grigorieva IV, Firsov AA (2004) Electric field effect in atomically thin carbon films. science 306 (5696):666-669
21. Novoselov KS, Jiang D, Schedin F, Booth T, Khotkevich V, Morozov S, Geim AK (2005) Two-dimensional atomic crystals. Proceedings of the National Academy of Sciences 102 (30):10451-10453
22. Guerra V, Wan C, McNally T (2019) Thermal conductivity of 2D nano-structured boron nitride (BN) and its composites with polymers. Progress in Materials Science 100:170-186
23. Li J-l, Yin J-h, Ji T, Feng Y, Liu Y-y, Zhao H, Li Y-p, Zhu C-c, Yue D, Su B (2019) Microstructure evolution effect on high-temperature thermal conductivity of LDPE/BNNS investigated by in-situ SAXS. Materials Letters 234:74-78
24. Yang X, Guo Y, Han Y, Li Y, Ma T, Chen M, Kong J, Zhu J, Gu J (2019) Significant improvement of thermal conductivities for BNNS/PVA composite films via electrospinning followed by hot-pressing technology. Composites Part B: Engineering 175:107070
25. Zhi C, Bando Y, Tang C, Kuwahara H, Golberg D (2009) Large-scale fabrication of boron nitride nanosheets and their utilization in polymeric composites with improved thermal and mechanical properties. Advanced Materials 21 (28):2889-2893
26. Watanabe K, Taniguchi T, Kanda H (2004) Direct-bandgap properties and evidence for ultraviolet lasing of hexagonal boron nitride single crystal. Nature materials 3 (6):404-409
27. Lin Y, Connell JW (2012) Advances in 2D boron nitride nanostructures: nanosheets, nanoribbons, nanomeshes, and hybrids with graphene. Nanoscale 4 (22):6908-6939
28. Doust Mohammadi M, Abdullah HY (2020) The Adsorption of Chlorofluoromethane on Pristine, Al-, Ga-, P-, and As-doped Boron Nitride Nanotubes: A PBC-DFT, NBO, and QTAIM Study. ChemistrySelect 5 (39):12115-12124
29. Doust Mohammadi M, Abdullah HY (2020) Adsorption of 1-chloro-1, 2, 2, 2-tetrafluoroethane on pristine, Al, Ga-doped boron nitride nanotubes: a study involving PBC-DFT, NBO analysis, and QTAIM. Canadian Journal of Chemistry 99:51-62
30. Mohammadi MD, Abdullah HY (2020) The adsorption of chlorofluoromethane on pristine, and Al-and Ga-doped boron nitride nanosheets: a DFT, NBO, and QTAIM study. Journal of Molecular Modeling 26 (10):287
31. Mohammadi MD, Abdullah HY (2020) Theoretical study of the adsorption of amantadine on pristine, Al-, Ga-, P-, and As-doped boron nitride nanosheets: a PBC-DFT, NBO, and QTAIM study. Theoretical Chemistry Accounts 139 (10):1-17
32. Mohammadi MD, Abdullah HY (2021) The adsorption of bromochlorodifluoromethane on pristine and Ge-doped silicon carbide nanotube: a PBC-DFT, NBO, and QTAIM study. Structural Chemistry 32:481-494
33. Mohammadi MD, Abdullah HY (2021) The adsorption of Bromochlorodifluoromethane on Pristine, Al, Ga, P, and As-doped Boron Nitride Nanotubes: A Study Involving PBC-DFT, NBO Analysis, and QTAIM. Computational and Theoretical Chemistry 1193:113047
34. Mohammadi MD, Salih IH, Abdullah HY (2020) An Ultimate Investigation on the Adsorption of Amantadine on Pristine and Decorated Fullerenes C59X (X= Si, Ge, B, Al, Ga, N, P, and As): A DFT, NBO, and QTAIM Study. Journal of Computational Biophysics and Chemistry 20:23-29
35. Mohammadi MD, Salih IH, Abdullah HY (2020) The adsorption of chlorofluoromethane on pristine and Ge-doped silicon carbide nanotube: a PBC-DFT, NBO, and QTAIM study. Molecular Simulation 46:1405-1416
36. Nemati-Kande E, Abbasi M, Mohammadi MD (2020) DFT studies on the interactions of pristine, Al and Ga-doped boron nitride nanosheets with CH3X (X= F, Cl and Br). Journal of Molecular Structure 1199:126962
37. Mohammadi MD, Abdullah HY, Bhowmick S, Biskos G (2021) Theoretical investigation of X12O12 (X= Be, Mg, and Ca) in sensing CH2N2: A DFT study. Computational and Theoretical Chemistry 1198:113168

38. Mohammadi MD, Abdullah HY, Bhowmick S, Biskos G (2021) A comprehensive investigation of the intermolecular interactions between CH2N2 and X12Y12 (X = B, Al, Ga; Y = N, P, As) nanocages. Canadian Journal of Chemistry 0 (0):1-9. doi:10.1139/cjc-2020-0473
39. Mohammadi MD, Abdullah HY (2021) Vinyl chloride adsorption onto the surface of pristine, Al-, and Ga-doped boron nitride nanotube: A DFT study. Solid State Communications 3379:114440
40. Peer D, Karp JM, Hong S, Farokhzad OC, Margalit R, Langer R (2020) Nanocarriers as an emerging platform for cancer therapy. Nano-Enabled Medical Applications:61-91
41. Rad AS, Aghaei SM (2018) Potential of metal–fullerene hybrids as strong nanocarriers for cytosine and guanine nucleobases: a detailed DFT study. Current Applied Physics 18 (2):133-140
42. Torchilin VP (2012) Multifunctional nanocarriers. Advanced drug delivery reviews 64:302-315
43. Schlegel HB (1982) Optimization of equilibrium geometries and transition structures. Journal of computational chemistry 3 (2):214-218
44. Perdew JP, Ernzerhof M, Burke K (1996) Rationale for mixing exact exchange with density functional approximations. The Journal of chemical physics 105 (22):9982-9985
45. Adamo C, Barone V (1999) Toward reliable density functional methods without adjustable parameters: The PBE0 model. The Journal of chemical physics 110 (13):6158-6170
46. Perdew JP, Burke K, Ernzerhof M (1996) Generalized gradient approximation made simple. Physical review letters 77 (18):3865
47. Zhao Y, Truhlar DG (2008) The M06 suite of density functionals for main group thermochemistry, thermochemical kinetics, noncovalent interactions, excited states, and transition elements: two new functionals and systematic testing of four M06-class functionals and 12 other functionals. Theoretical chemistry accounts 120 (1):215-241
48. Zhao Y, Truhlar DG (2006) Density functional for spectroscopy: no long-range self-interaction error, good performance for Rydberg and charge-transfer states, and better performance on average than B3LYP for ground states. The Journal of Physical Chemistry A 110 (49):13126-13130
49. Chai J-D, Head-Gordon M (2008) Long-range corrected hybrid density functionals with damped atom–atom dispersion corrections. Physical Chemistry Chemical Physics 10 (44):6615-6620
50. Grimme S (2006) Semiempirical GGA-type density functional constructed with a long-range dispersion correction. Journal of computational chemistry 27 (15):1787-1799
51. Grimme S, Antony J, Ehrlich S, Krieg H (2010) A consistent and accurate ab initio parametrization of density functional dispersion correction (DFT-D) for the 94 elements H-Pu. The Journal of chemical physics 132 (15):154104
52. Grimme S, Ehrlich S, Goerigk L (2011) Effect of the damping function in dispersion corrected density functional theory. Journal of computational chemistry 32 (7):1456-1465
53. Frisch MJ, Trucks GW, Schlegel HB, Scuseria GE, Robb MA, Cheeseman JR, Scalmani G, Barone V, Petersson GA, Nakatsuji H, Li X, Caricato M, Marenich AV, Bloino J, Janesko BG, Gomperts R, Mennucci B, Hratchian HP, Ortiz JV, Izmaylov AF, Sonnenberg JL, Williams, Ding F, Lipparini F, Egidi F, Goings J, Peng B, Petrone A, Henderson T, Ranasinghe D, Zakrzewski VG, Gao J, Rega N, Zheng G, Liang W, Hada M, Ehara M, Toyota K, Fukuda R, Hasegawa J, Ishida M, Nakajima T, Honda Y, Kitao O, Nakai H, Vreven T, Throssell K, Montgomery Jr. JA, Peralta JE, Ogliaro F, Bearpark MJ, Heyd JJ, Brothers EN, Kudin KN, Staroverov VN, Keith TA, Kobayashi R, Normand J, Raghavachari K, Rendell AP, Burant JC, Iyengar SS, Tomasi J, Cossi M, Millam JM, Klene M, Adamo C, Cammi R, Ochterski JW, Martin RL, Morokuma K, Farkas O, Foresman JB, Fox DJ (2016) Gaussian 16 Rev. C.01. Wallingford, CT
54. Binning Jr R, Curtiss L (1990) Compact contracted basis sets for third-row atoms: Ga–Kr. Journal of Computational Chemistry 11 (10):1206-1216
55. Curtiss LA, McGrath MP, Blaudeau JP, Davis NE, Binning Jr RC, Radom L (1995) Extension of Gaussian-2 theory to molecules containing third-row atoms Ga–Kr. The Journal of Chemical Physics 103 (14):6104-6113

689 56. Frisch MJ, Pople JA, Binkley JS (1984) Self-consistent molecular orbital methods 25. Supplementary
690 functions for Gaussian basis sets. The Journal of chemical physics 80 (7):3265-3269
691 57. Hay PJ (1977) Gaussian basis sets for molecular calculations. The representation of 3 d orbitals in
692 transition-metal atoms. The Journal of Chemical Physics 66 (10):4377-4384
693 58. J.-P. Blaudeau MPM, L. A. Curtiss, and L. Radom (1997) Extension of Gaussian-2 (G2) theory to
694 molecules containing third-row atoms K and Ca. J Chem Phys 107:5016-5021
695 59. K. Raghavachari JSB, R. Seeger, and J. A. Pople (1980) Self-Consistent Molecular Orbital Methods. 20.
696 Basis set for correlated wave-functions. J Chem Phys 72 650-654
697 60. McGrath MP, Radom L (1991) Extension of Gaussian-1 (G1) theory to bromine-containing molecules.
698 The Journal of Chemical Physics 94 (1):511-516
699 61. Raghavachari K, Trucks GW (1989) Highly correlated systems. Excitation energies of first row
700 transition metals Sc–Cu. The Journal of chemical physics 91 (2):1062-1065
701 62. Russo TV, Martin RL, Hay PJ (1994) Density functional calculations on first-row transition metals. The
702 Journal of chemical physics 101 (9):7729-7737
703 63. Goerigk L, Grimme S (2011) A thorough benchmark of density functional methods for general main
704 group thermochemistry, kinetics, and noncovalent interactions. Physical Chemistry Chemical Physics 13
705 (14):6670-6688
706 64. Mardirossian N, Head-Gordon M (2017) Thirty years of density functional theory in computational
707 chemistry: an overview and extensive assessment of 200 density functionals. Molecular Physics 115
708 (19):2315-2372
709 65. Brakestad A, Jensen SR, Wind P, D'Alessandro M, Genovese L, Hopmann KH, Frediani L (2020) Static
710 polarizabilities at the basis set limit: A benchmark of 124 species. Journal of chemical theory and
711 computation 16 (8):4874-4882
712 66. Mitra H, Roy TK (2020) Comprehensive Benchmark Results for the Accuracy of Basis Sets for
713 Anharmonic Molecular Vibrations. The Journal of Physical Chemistry A 124 (44):9203-9221
714 67. Goerigk L, Hansen A, Bauer C, Ehrlich S, Najibi A, Grimme S (2017) A look at the density functional
715 theory zoo with the advanced GMTKN55 database for general main group thermochemistry, kinetics
716 and noncovalent interactions. Physical Chemistry Chemical Physics 19 (48):32184-32215
717 68. Dennington R, Keith TA, Millam JM (2016) GaussView, version 6.0. 16. Semichem Inc Shawnee
718 Mission KS
719 69. Andrienko G (2010) Chemcraft. Graphical Software for Visualization of Quantum Chemistry
720 Computations. https://www.chemcraftprog.com,
721 70. Foster aJ, Weinhold F (1980) Natural hybrid orbitals. Journal of the American Chemical Society 102
722 (24):7211-7218
723 71. Reed AE, Weinhold F (1983) Natural bond orbital analysis of near-Hartree–Fock water dimer. The
724 Journal of chemical physics 78 (6):4066-4073
725 72. Carpenter J, Weinhold F (1988) Analysis of the geometry of the hydroxymethyl radical by the
726 "different hybrids for different spins" natural bond orbital procedure. Journal of Molecular Structure:
727 THEOCHEM 169:41-62
728 73. Lu T, Chen F (2012) Multiwfn: a multifunctional wavefunction analyzer. Journal of computational
729 chemistry 33 (5):580-592
730 74. O'boyle NM, Tenderholt AL, Langner KM (2008) Cclib: a library for package-independent
731 computational chemistry algorithms. Journal of computational chemistry 29 (5):839-845
732 75. Mayer I, Valiron P (1998) Second order Mo/ller–Plesset perturbation theory without basis set
733 superposition error. The Journal of chemical physics 109 (9):3360-3373
734 76. Boys SF, Bernardi F (1970) The calculation of small molecular interactions by the differences of
735 separate total energies. Some procedures with reduced errors. Molecular Physics 19 (4):553-566

77. Alkorta I, Trujillo C, Elguero J, Solimannejad M (2011) A theoretical study of the hydrogen bonding properties of H2BNH2: Some considerations on the basis set superposition error issue. Computational and Theoretical Chemistry 967 (1):147-151
78. Thomas LH The calculation of atomic fields. In: Mathematical proceedings of the Cambridge philosophical society, 1927. vol 5. Cambridge University Press, pp 542-548
79. Fermi E (1927) Statistical method to determine some properties of atoms. Rend Accad Naz Lincei 6 (602-607):5
80. Dirac PA Note on exchange phenomena in the Thomas atom. In: Mathematical proceedings of the Cambridge philosophical society, 1930. vol 3. Cambridge University Press, pp 376-385
81. Slater JC (1951) A simplification of the Hartree-Fock method. Physical review 81 (3):385
82. Hohenberg P, Kohn W (1964) Inhomogeneous electron gas. Physical review 136 (3B):B864
83. Kohn W, Sham LJ (1965) Self-consistent equations including exchange and correlation effects. Physical review 140 (4A):A1133
84. Becke AD (2014) Perspective: Fifty years of density-functional theory in chemical physics. The Journal of chemical physics 140 (18):18A301
85. Burke K, Wagner LO (2013) DFT in a nutshell. International Journal of Quantum Chemistry 113 (2):96-101
86. Becke AD (1988) Density-functional exchange-energy approximation with correct asymptotic behavior. Physical review A 38 (6):3098
87. Gill PM (1996) A new gradient-corrected exchange functional. Molecular Physics 89 (2):433-445
88. Vosko SH, Wilk L, Nusair M (1980) Accurate spin-dependent electron liquid correlation energies for local spin density calculations: a critical analysis. Canadian Journal of physics 58 (8):1200-1211
89. Perdew JP (1986) Density-functional approximation for the correlation energy of the inhomogeneous electron gas. Physical Review B 33 (12):8822
90. Lee C, Yang W, Parr RG (1988) Development of the Colle-Salvetti correlation-energy formula into a functional of the electron density. Physical review B 37 (2):785
91. Perdew JP, Zunger A (1981) Self-interaction correction to density-functional approximations for many-electron systems. Physical Review B 23 (10):5048
92. Cole LA, Perdew J (1982) Calculated electron affinities of the elements. Physical Review A 25 (3):1265
93. Perdew JP, Wang Y (1992) Accurate and simple analytic representation of the electron-gas correlation energy. Physical review B 45 (23):13244
94. Becke AD (1997) Density-functional thermochemistry. V. Systematic optimization of exchange-correlation functionals. The Journal of chemical physics 107 (20):8554-8560
95. Perdew JP, Chevary JA, Vosko SH, Jackson KA, Pederson MR, Singh DJ, Fiolhais C (1992) Atoms, molecules, solids, and surfaces: Applications of the generalized gradient approximation for exchange and correlation. Physical review B 46 (11):6671
96. Paier J, Marsman M, Kresse G (2007) Why does the B3LYP hybrid functional fail for metals? The Journal of chemical physics 127 (2):024103
97. Yanai T, Tew DP, Handy NC (2004) A new hybrid exchange–correlation functional using the Coulomb-attenuating method (CAM-B3LYP). Chemical physics letters 393 (1-3):51-57
98. Leininger T, Stoll H, Werner H-J, Savin A (1997) Combining long-range configuration interaction with short-range density functionals. Chemical physics letters 275 (3-4):151-160
99. Bhatta RS, Pellicane G, Tsige M (2015) Tuning range-separated DFT functionals for accurate orbital energy modeling of conjugated molecules. Computational and Theoretical Chemistry 1070:14-20
100. Sekar N, Katariya S, Rhyman L, Alswaidan IA, Ramasami P (2019) Molecular and NLO Properties of Red Fluorescent Coumarins–DFT Computations Using Long-Range Separated and Conventional Functionals. Journal of fluorescence 29 (1):241-253

101. Tao J, Perdew JP, Staroverov VN, Scuseria GE (2003) Climbing the density functional ladder: Nonempirical meta–generalized gradient approximation designed for molecules and solids. Physical Review Letters 91 (14):146401
102. PubChem database, https://pubchem.ncbi.nlm.nih.gov/, 2021.
103. Kohl D (1990) The role of noble metals in the chemistry of solid-state gas sensors. Sensors and Actuators B: Chemical 1 (1-6):158-165
104. Foresman JB, Frisch A (1996) Exploring chemistry with electronic structure methods: a guide to using Gaussian.
105. Mohammadi Md, Abdullah Hy, Biskos G, Bhowmick S (2021) Enhancing the absorption of 1-chloro-1, 2, 2, 2-tetrafluoroethane on carbon nanotubes: an ab initio study. Bulletin of Materials Science, 44(2021) 198.
106. Mohammadi MD, Abdullah HY, Suvitha A (2021) The Adsorption of 1-Chloro-1,2,2,2-Tetrafluoroethane Onto the Pristine, Al-, and Ga-Doped Boron Nitride Nanosheet. Iranian Journal of Science and Technology, Transactions A: Science 45 (2021) 1287–1300
107. Geerlings P, De Proft F, Langenaeker W (2003) Conceptual density functional theory. Chemical reviews 103 (5):1793-1874
108. Islam N, Kaya S (2018) Conceptual density functional theory and its application in the chemical domain. CRC Press,
109. Chermette H (1999) Chemical reactivity indexes in density functional theory. Journal of computational chemistry 20 (1):129-154
110. Pearson RG (2005) Chemical hardness and density functional theory. Journal of Chemical Sciences 117 (5):369-377
111. Ayers PW, Anderson JS, Bartolotti LJ (2005) Perturbative perspectives on the chemical reaction prediction problem. International Journal of Quantum Chemistry 101 (5):520-534
112. Bultinck P, Cardenas C, Fuentealba P, Johnson PA, Ayers PW (2013) Atomic charges and the electrostatic potential are ill-defined in degenerate ground states. Journal of chemical theory and computation 9 (11):4779-4788
113. Bultinck P, Cardenas C, Fuentealba P, Johnson PA, Ayers PW (2014) How to compute the Fukui matrix and function for systems with (quasi-) degenerate states. Journal of chemical theory and computation 10 (1):202-210
114. Parr RG, Donnelly RA, Levy M, Palke WE (1978) Electronegativity: the density functional viewpoint. The Journal of Chemical Physics 68 (8):3801-3807
115. Parr RG, Pearson RG (1983) Absolute hardness: companion parameter to absolute electronegativity. Journal of the American chemical society 105 (26):7512-7516
116. Parr RG, Yang W (1984) Density functional approach to the frontier-electron theory of chemical reactivity. Journal of the American Chemical Society 106 (14):4049-4050
117. Yang W, Parr RG, Pucci R (1984) Electron density, Kohn–Sham frontier orbitals, and Fukui functions. The Journal of Chemical Physics 81 (6):2862-2863
118. Morell C, Grand A, Toro-Labbe A (2005) New dual descriptor for chemical reactivity. The Journal of Physical Chemistry A 109 (1):205-212
119. Levy M (1982) Electron densities in search of Hamiltonians. Physical Review A 26 (3):1200
120. Parr RG, Szentpály Lv, Liu S (1999) Electrophilicity index. Journal of the American Chemical Society 121 (9):1922-1924
121. Bredas J-L (2014) Mind the gap! Materials Horizons 1 (1):17-19
122. Koopmans T (1934) Über die Zuordnung von Wellenfunktionen und Eigenwerten zu den einzelnen Elektronen eines Atoms. physica 1 (1-6):104-113
123. Janak J (1978) Proof thatð eð n i= ε in density-functional theory. Physical Review B 18 (12):7165

124. Schmidt MW, Hull EA, Windus TL (2015) Valence virtual orbitals: An unambiguous ab initio quantification of the LUMO concept. The Journal of Physical Chemistry A 119 (41):10408-10427
125. Mulliken RS (1932) Electronic structures of polyatomic molecules and valence. II. General considerations. Physical Review 41 (1):49
126. Löwdin P-O (1955) Quantum theory of many-particle systems. I. Physical interpretations by means of density matrices, natural spin-orbitals, and convergence problems in the method of configurational interaction. Physical Review 97 (6):1474
127. Coulson CA (1939) The electronic structure of some polyenes and aromatic molecules. VII. Bonds of fractional order by the molecular orbital method. Proceedings of the Royal Society of London Series A Mathematical and Physical Sciences 169 (938):413-428
128. Mulliken RS (1955) Electronic population analysis on LCAO–MO molecular wave functions. I. The Journal of Chemical Physics 23 (10):1833-1840
129. Mayer I (1983) Charge, bond order and valence in the AB initio SCF theory. Chemical Physics Letters 97 (3):270-274
130. Mayer I (2012) Improved definition of bond orders for correlated wave functions. Chemical Physics Letters 544:83-86
131. Bridgeman AJ, Cavigliasso G, Ireland LR, Rothery J (2001) The Mayer bond order as a tool in inorganic chemistry. Journal of the Chemical Society, Dalton Transactions (14):2095-2108
132. Wiberg KB (1968) Application of the pople-santry-segal CNDO method to the cyclopropylcarbinyl and cyclobutyl cation and to bicyclobutane. Tetrahedron 24 (3):1083-1096
133. Sizova OV, Skripnikov LV, Sokolov AY (2008) Symmetry decomposition of quantum chemical bond orders. Journal of Molecular Structure: THEOCHEM 870 (1-3):1-9
134. Bader RF (1985) Atoms in molecules. Accounts of Chemical Research 18 (1):9-15
135. Bader R (1990) A Quantum Theory, Clarendon. Oxford,
136. Bader RFW, Popelier PLA, Keith TA (1994) Theoretical definition of a functional group and the molecular orbital paradigm. Angewandte Chemie International Edition in English 33 (6):620-631
137. Matta CF (2006) Hydrogen–hydrogen bonding: the non-electrostatic limit of closed-shell interaction between two hydro. In: Hydrogen Bonding—New Insights. Springer, pp 337-375
138. Grabowski SJ (2012) QTAIM characteristics of halogen bond and related interactions. The Journal of Physical Chemistry A 116 (7):1838-1845
139. Bohórquez HJ, Boyd RJ, Matta CF (2011) Molecular model with quantum mechanical bonding information. The Journal of Physical Chemistry A 115 (45):12991-12997
140. Johnson ER, Keinan S, Mori-Sánchez P, Contreras-García J, Cohen AJ, Yang W (2010) Revealing noncovalent interactions. Journal of the American Chemical Society 132 (18):6498-6506
141. Contreras-García J, Johnson ER, Keinan S, Chaudret R, Piquemal J-P, Beratan DN, Yang W (2011) NCIPLOT: a program for plotting noncovalent interaction regions. Journal of chemical theory and computation 7 (3):625-632